DOI: 10.1002/adma.200701085

Al-Doped TiO_2 Films with Ultralow Leakage Currents for Next Generation DRAM Capacitors**

By *Seong Keun Kim, Gyu-Jin Choi, Sang Young Lee, Minha Seo, Sang Woon Lee, Jeong Hwan Han, Hyo-Shin Ahn, Seungwu Han,* and *Cheol Seong Hwang**

Dynamic random access memory (DRAM) is used as the main memory of every modern computer, due to its high density, high speed and efficient memory function. Each DRAM cell consists of one transistor, which functions as a switch for the stored charge, and one capacitor where the positive or negative electric charges corresponding to the digital 1 or 0 data are stored (see Fig. 1a). For successful operation of DRAM, a large cell capacitance (~25 fF) and low leakage current at the operation voltage (10^{-7} A cm^{-2} or 1 fA/cell) are required because of the following reasons; during the reading operation, stored charge is shared between the cell capacitor and bit line, which is connected to the sense amplifier. In modern DRAMs, hundreds of capacitors are connected to one bit-line so that the bit-line capacitance is usually a few ten times larger than that of the capacitor. Therefore, for a bit-line voltage variation of ~100 mV through the charge sharing, which is the sensing margin of the circuit, at least ~25 fF of cell capacitance is necessary.[1–3] The low leakage current is also essential to ensure a sufficient refresh time.

In a traditional Si-based capacitor, the target cell capacitance has been achieved by increasing the surface area of the capacitor (semiconductor-insulator-semiconductor, SIS, in Fig. 1b) while the dielectric thickness is scaled down according to the design rules.[4] More recently, innovations have been made in the component materials. A metal electrode, TiN or Ru, and a dielectric material with a higher-k value (k is the relative dielectric constant) than that of the SiO_2/Si_3N_4 layer ($k \sim 6$–7), such as HfO_2 ($k \sim 25$),[5,6] ZrO_2 ($k \sim 40$)[7] and Ta_2O_5 ($k \sim 25$–60)[8,9] are being explored in giga-bit scale DRAMs (metal-insulator-semiconductor, MIS, and metal-insulator-metal, MIM, in Fig. 1b). The ability of a dielectric film to store charge is conveniently represented by the equivalent oxide thickness ($t_{ox}, = t_{phy} \times 3.9/k$, where t_{phy} is the physical thickness of the film). The minimum achievable t_{ox} is ~0.7 nm for HfO_2, ZrO_2 and Ta_2O_5 which are currently being used in the DRAM industry. However, the technology road map for memory devices states that t_{ox} less than 0.5 nm is necessary for the DRAMs with a design rule of <40 nm.[10] It is also noted that there are no known material solutions to serve this purpose. Reducing the thickness of the dielectric films with k values ~20–30 to achieve the required t_{ox} results in unacceptably high leakage currents. Therefore, a dielectric material with a higher k value is in demand. Perovskite-based dielectric films such as $SrTiO_3$[11,12] and $(Ba,Sr)TiO_3$[13] were reported to exhibit k values of several hundreds and therefore t_{ox} of ~0.24 nm is feasible with these materials.[14] However, growth of these films is extremely difficult with the atomic-layer-deposition (ALD) which is a method of choice for the growth of the dielectric films in microelectronic devices. A low thermal budget of 500–600 °C during the deposition and post-deposition annealing (PDA) processes is another key concern against employing perovskite oxides.

In this article, the authors report Al-doped TiO_2 (ATO) dielectric thin films grown by an ALD method for application to next-generation DRAM capacitors. Although the TiO_2 film having Al is termed as the Al-doped TiO_2 films for the sake of simplicity, it would be better to understand the material as the Al_2O_3-doped TiO_2. TiO_2 thin film in rutile phase exhibits a k value ~100[15,16] and therefore can be used for DRAMs with a design rule of <40 nm. However, the small energy gap of 3.1 eV implies that the control of leakage currents is not trivial. The authors achieve the specifications on the leakage currents, that is, 10^{-7} A cm^{-2} at 0.8 V, through elaborate doping of TiO_2 films with Al atoms. In addition, it was found that this specific thin film material and process can meet all of the critical requirements discussed above. Therefore, this material and process appear to provide the DRAM industry with a new way to resolve one of the most crucial problems in pursuing further higher density DRAMs while remaining in the same trend as before without invoking a fundamentally different paradigm.

Growth of Al-doped TiO_2 thin films by ALD. The authors recently reported that rutile structured TiO_2 film with a higher k (>80) was grown on a Ru electrode at 250 °C, due to the structural compatibility between the in situ formed RuO_2 at the interface during the ALD of TiO_2 using O_3 and rutile

[*] Prof. C. S. Hwang, Dr. S. K. Kim, G.-J. Choi, S. Y. Lee, M. Seo
S. W. Lee, J. H. Han
Department of Materials Science and Engineering and
Inter-university Semiconductor Research Center
Seoul National University
Seoul, 151-744 (Korea)
E-mail: cheolsh@snu.ac.kr

Dr. H.-S. Ahn, Prof. S. Han
Department of Physics
Ewha Woman's University
Seoul, 120-750 (Korea)

[**] The work was supported by the System IC 2010 program of the Korean government. The authors would like to acknowledge fruitful discussions with S. Hoffmann-Eifert at Forschungszentrum Jülich. Supporting Information is available online from Wiley InterScience or from the author.

 © 2008 WILEY-VCH Verlag GmbH & Co. KGaA,Weinheim WILEY InterScience DISCOVER SOMETHING GREAT

ADVANCED MATERIALS

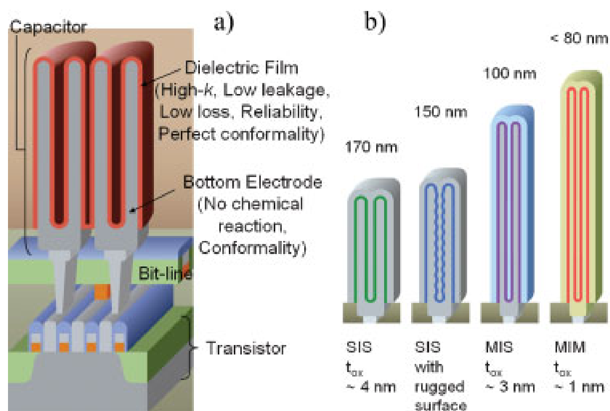

Figure 1. (a) Schematic diagram of DRAM cells which consist of a cell transistor and capacitor. (b) A summary of the DRAM capacitor technology evolution.

TiO_2.[15,17] This k value of ~80 is the highest value reported from simple binary oxide films having a thickness of ~10 nm. In addition, it was reported that TiO_2 films grown by ALD showed superior conformality in their dielectric properties as well as their film thickness in contact hole structured capacitors.[18] Ru electrodes, which were used in previous studies, are very promising as the capacitor electrode of future DRAMs because the adoption of a noble metal can remove the low-k interfacial layer and the conformal deposition of Ru films on severe contact hole structures can also be achieved.[19]

Although the rutile-structured TiO_2 films fabricated on the Ru electrode showed a k value high enough to be employed in future DRAMs, the leakage current level is unacceptably high. Therefore, the achievable minimum t_{ox} remained ~0.8 nm for a given condition of the leakage current density, that is, $<10^{-7}$ A cm^{-2} at 0.8 V. From the fundamental point of view, this is mainly attributed to the small energy gap of TiO_2; rutile TiO_2 has a band gap of ~3.1 eV. Therefore, the maximum conduction and valence band offset with respect to the Fermi level of the metal electrode is 1.55 eV, which is actually not too small a value to suppress the thermionic emission of electrons from the metal Fermi level to the conduction band of TiO_2. However, TiO_2 films usually have n-type characteristics due to the presence of oxygen vacancies or titanium interstitials in the film, suggesting that the conduction band offset (the energy difference between the Fermi level of the electrode and the conduction band edge of TiO_2) is reduced. In addition, the charge neutrality level of TiO_2 lies closer to the conduction band.[20] Due to the small energy gap, a slight change of offset can increase the leakage current greatly. In this study, as a simple idea to compensate for the n-type nature of TiO_2 thin film, Al ions as an acceptor are doped into the TiO_2 films.

The overall [Al]/[Al+Ti] atomic ratios of the ATO films with R_{pc} values (see Experimental) of 1/60, 1/90, and 1/120 are 12, 8, and 6 at%, respectively, measured by an inductively coupled plasma spectroscopy-atomic emission spectrometer (ICP-AES), as shown in Figure 2a. In this study, an Al-O layer was discretely introduced into the film due to the pulse-cycling nature of ALD. However, the Al ions are distributed uniformly along the thickness direction, as shown by the composition depth profile of the sample with the R_{pc} of 1/120 obtained by Auger electron spectroscopy (inset in Fig. 2a). One notable finding from Figure 2a is the higher Al concentration measured by X-ray photoelectron spectroscopy (XPS), which is surface sensitive, as compared to that measured by ICP-AES, which probes the whole thickness of the film. The high Al concentration obtained from XPS suggests that the Al ions segregate to the film surface. This corresponds well to the first-principles calculation shown later in this report. The Al ions find energetically favorable positions on the rutile TiO_2 surface, which greatly contributes to the improvement in the electrical properties.

XPS was also used to investigate the chemical bindings of the ATO films. The inset figures in Figure 2b show the Ti2p, and O$1s$ XPS spectra of the TiO_2 and ATO films and Figure 2b shows the binding energy spacing between the O$1s$ and Ti2p peaks as a function of the R_{pc} value. The Ti2p and Al2p (data not shown) core level spectra of the ATO films show only a single component. Although the O$1s$ core level spectra did not show a symmetric shape, the major component near a binding energy of 530.0 eV may correspond to bonding with Ti and Al. The other components near the binding energies of 531.2 and 532.2 eV may mainly correspond to hydrated bonds or carbonate caused by contamination on the film surface. The oxygen and titanium in each condition must be present in one binding state, because the simultaneous

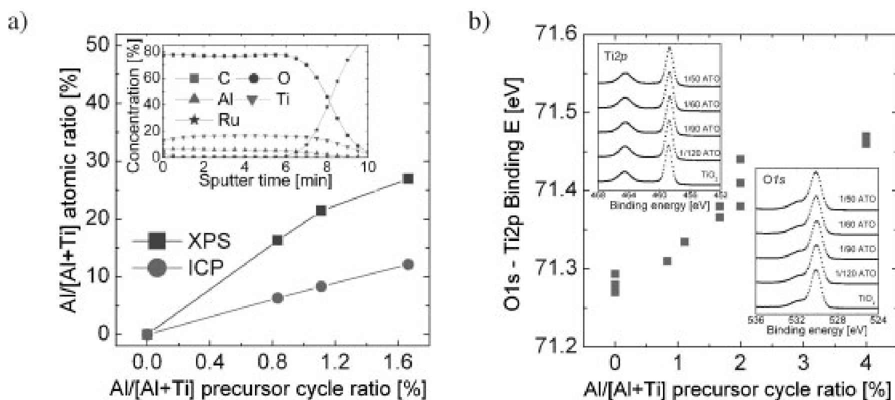

Figure 2. (a) Al/[Al+Ti] atomic ratio of the ATO films measured by XPS and ICP-AES as a function of the Al/[Al+Ti] precursor cycle ratio. Inset figure shows AES depth profile of ATO film. (b) The energy spacing between the O$1s$ and Ti$2p$ peaks as a function of the Al/[Al+Ti] precursor cycle ratio. Inset figures show Ti$2p$, and O$1s$ XPS spectra of TiO_2 and ATO films.

© 2008 WILEY-VCH Verlag GmbH & Co. KGaA, Weinheim

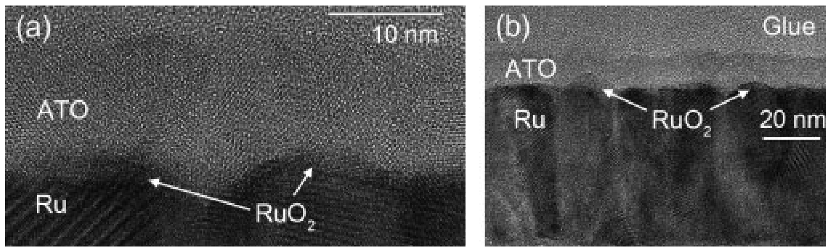

Figure 3. (a) HRTEM image of ATO film on Ru electrode. (b) TEM image with a lower magnification of ATO film on Ru electrode.

existence of the two binding states O–Ti and O–Al would otherwise have been resolved in the XP spectra.[21] The energy spacing between the O*1s* and Ti*2p* peaks slightly increased with increasing R_{pc} value from 71.25 to 71.50 eV. Richthofen et al. reported a similar trend in Ti–Al–O films prepared by reactive magnetron sputtered ion plating.[21] They confirmed the wide range of solid solubility between Al_2O_3 and TiO_2 under non-equilibrium conditions from the continuous shift of the kinetic energy of the O-KLL Auger spectra between the two binary phases. In addition, Zheng et al.[22] reported that the Ti*2p* peak of BST film was shifted to a low binding energy by the incorporation of Al_2O_3 into the film, due to the charge transfer effect. Therefore, the results shown in Figure 2b suggest that the Al ions in the film form a chemically uniform Al–Ti–O film without any phase separation.

The micro-structural uniformity of the film was investigated by high-resolution transmission electron microscopy (HRTEM). Figure 3a shows the HRTEM image of ATO/Ru. The ATO/Ru interface barely shows the RuO_2 due to its thin thickness and overlap of its contrast with the images of Ru and ATO. Lattice fringes in the ATO film layer are clearly shown. However, a clear identification of the phase, anatase or rutile, was not probable from this image due to the similar lattice spacing of the two phases. X-ray diffraction was not effective at this thickness of the film either. However, the higher *k* value, shown below, suggests that the film should be of the rutile structure. TEM with a lower magnification (Fig. 3b) confirms the smooth surface and uniform thickness over a large area without showing any signature of the phase separation.

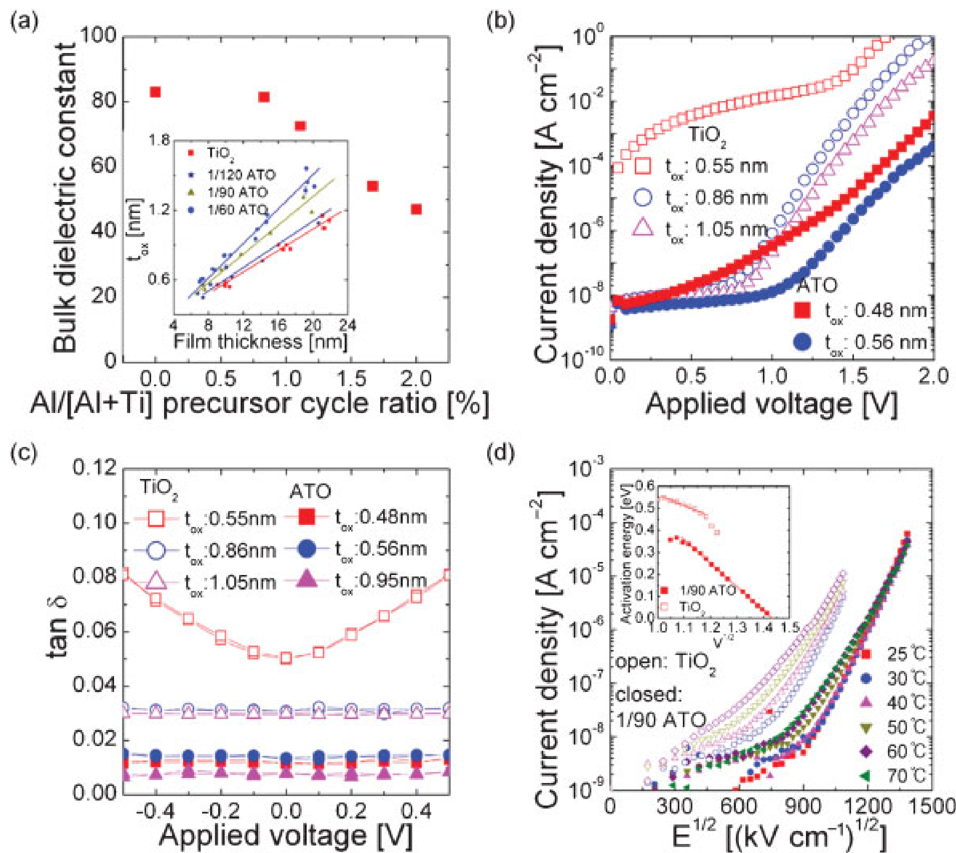

Figure 4. (a) Bulk dielectric constant of TiO_2 and ATO films as a function of the Al/[Al+Ti] precursor cycle ratio. Inset figure shows the variation in the t_{ox} of the films as a function of the film thickness. (b) J–V curves of TiO_2 and ATO films. (c) The dielectric loss (tan δ) versus voltage graphs of the TiO_2 and ATO films. (d) $J - E^{\frac{1}{2}}$ characteristics of the TiO_2 and ATO films at temperatures ranging from 25 to 70 °C. The inset figure shows the variation in the activation energy as a function of the $V^{\frac{1}{2}}$ of the TiO_2 and ATO films.

© 2008 WILEY-VCH Verlag GmbH & Co. KGaA,Weinheim

ADVANCED MATERIALS

Electrical properties of Al-doped TiO_2 films. The variations in the t_{ox} of the ATO films with various R_{pc} values as a function of the film thickness are shown in the inset figure of Figure 4a. The variations in the t_{ox} of the un-doped TiO_2 films are also illustrated for comparison. It can be seen that the y-intercepts of all of the graphs have positive values (inset figure of Fig. 4a). This is due to the presence of the low-k interfacial layer which is induced by the effects of the intrinsic dead layer[23,24] and electrode polarization due to the finite Thomas-Fermi screening length of the electrodes.[25,26] The segregation of Al to the surface may also contribute to the presence of the low-k interface layer. The possibility that the very thin surface and interface region (~1nm-thick) has an amorphous structure with a lower k value cannot be completely excluded considering the higher Al concentration and more disordered structure of the surface, although it was not clearly revealed by the HRTEM. This may also contribute to the presence of the interfacial capacitance shown in Figure 4a. The bulk k values of the films with the various R_{pc} values were calculated (Fig. 4a) from the slopes of the graphs of t_{ox} as a function of the film thickness, which excludes the influence of the interface. The bulk k values of the ATO films decreased with increasing R_{pc} value from 81 at an R_{pc} of 1/120 to 47 at an R_{pc} value of 1/50, possibly due to the low polarizability of the Ti–O–Al bond. The bulk k value of TiO_2 was 83. Although the dielectric constants of the ATO films are lower than those of the un-doped TiO_2 films, they are still higher than those of alternative dielectric binary oxides such as HfO_2, ZrO_2, and Ta_2O_5. It should also be noted that the k value of 47 is higher than that of un-doped anatase structured TiO_2.[15] In addition, the capacitance – voltage (C–V) curves of the ATO films showed absolutely flat behavior in the voltage region from −1 to 1 V, due to linear dielectric property of this material (data not shown). The flat behavior of the C–V curves is another crucial merit of ATO over $(Ba,Sr)TiO_3$.

The reduction of the leakage current by Al-doping was confirmed by measuring the current density – voltage (J–V) characteristics of the un-doped and Al-doped TiO_2 films. The J level in the bottom Ru (RuO_2) electrode injection condition (positive bias to the top Pt) was always higher than that in the case of the top Pt electrode injection (negative bias to the top Pt), so that only J–V characteristics with a positive bias to the top Pt electrode are reported. The reason for the higher J level in the bottom Ru (RuO_2) electrode injection condition might be the lower work function of RuO_2 (4.9 eV) compared to Pt (5.5 eV). The J–V behaviors of the un-doped TiO_2 (with t_{ox} values of 0.55, 0.86 and 1.05 nm, respectively) and ATO (with an R_{pc} value of 1/60 which shows t_{ox} values of 0.48 and 0.56 nm, respectively) films are shown in Figure 4b. It can be seen that a sufficiently low J level at 0.8 V ($<10^{-7}$ Acm^{-2}) was achieved when the t_{ox} is >0.86 nm for the un-doped TiO_2 film. However, at a t_{ox} of 0.55 nm, J abruptly increases to a few $mAcm^{-2}$. It was confirmed that the leakage properties of the films were remarkably improved by the doping of Al ions into them (decrease by $> \sim 10^5$ times at $t_{ox} \sim 0.5$–0.6 nm). In particular, a film with a t_{ox} of 0.48 nm and a low enough J level ($<10^{-7}$ Acm^{-2} at 0.8 V) was obtained. This t_{ox} value is ~28% lower than the smallest value reported for ZrO_2 film ($t_{ox} \sim 0.64$ nm).[7] This is a significant improvement since the low t_{ox} of the dielectric film is the most crucial factor for DRAM capacitors. Figure 4c shows the dielectric loss (tan δ) vs. voltage graphs of the un-doped TiO_2 and ATO films. The tan δ of the un-doped TiO_2 films is ~3% when the J level is low, but it substantially increases when the J level is high (t_{ox} of 0.55 nm). However, the tan δ of the ATO films decreases to 0.7–1.5%, which suggests that some of the dielectric loss mechanism is removed by the doping. This low level of tan δ is maintained at the minimum t_{ox} of 0.48 nm. A low value of tan δ is especially important for the fast charging and discharging of the capacitor (faster operation of DRAM).

To elucidate the reason for the remarkable improvement in the leakage current properties of the ATO films, the leakage conduction mechanism of Pt/TiO_2/Ru and Pt/ATO (R_{pc} of 1/90)/Ru capacitors was investigated. The J–V characteristics were measured at temperatures ranging from 25 to 70 °C under Pt injection conditions (negative bias to top Pt). The repeated J–V measurement under the positive bias condition at high temperatures induced the degradation of the resistance during the measurement and, thus, the more resistant negative bias J–V characteristics are compared. However, the same conclusion can be applied to the positive bias case. Figure 4d shows the $J - E^{1/2}$ characteristics of the TiO_2 and ATO thin films at various temperatures. It was again confirmed that the J level of the ATO film is much smaller than that of TiO_2 at all temperatures under this bias condition. The J value of the films increased linearly above $E^{1/2}$ values of ~700 and 900 $(kV\,cm^{-1})^{1/2}$ for the TiO_2 and ATO films, respectively, in the whole range of measured temperature. J also increases with increasing temperature in these E regions. This suggests that the leakage conduction of both films followed Schottky emission behavior at the film/electrode interface or the Poole-Frenkel mechanism due to the presence of bulk traps. The fitting of the experimental data set according to the Schottky emission or Poole-Frenkel theory showed that the Schottky emission was the proper mechanism to explain the J–V behaviors for both cases. The appropriateness of the Schottky model is confirmed by the coincidence between the extracted high-frequency k values from the Schottky fitting (7.7 and 5.8 for TiO_2 and ATO, respectively. Note that the large k (47–81) values shown in Figure 4a correspond to the low-frequency values.) and optical frequency dielectric constant of the films ($n^2 \sim 7.3$ and 6.3 for TiO_2 and ATO, respectively, where n is the refractive index measured by ellipsometry). Above an $E^{1/2}$ of 1300 $(kV\,cm^{-1})^{1/2}$, for the ATO case, the temperature dependence of the $J - E^{1/2}$ curve disappeared, suggesting that the leakage current mechanism of the film changes from Schottky emission to tunneling in this high E region. The interfacial potential barrier height (Φ_b), which is influenced by the image force effect, appears in the form of the activation energy at each bias V, and the extrapolation to $V = 0$ gives the Φ_b formed at the Pt/TiO_2 and Pt/ATO interfaces (inset figure of Fig. 4d). Φ_b for the Pt/TiO_2 and Pt/ATO films was 1.05 and

 © 2008 WILEY-VCH Verlag GmbH & Co. KGaA,Weinheim

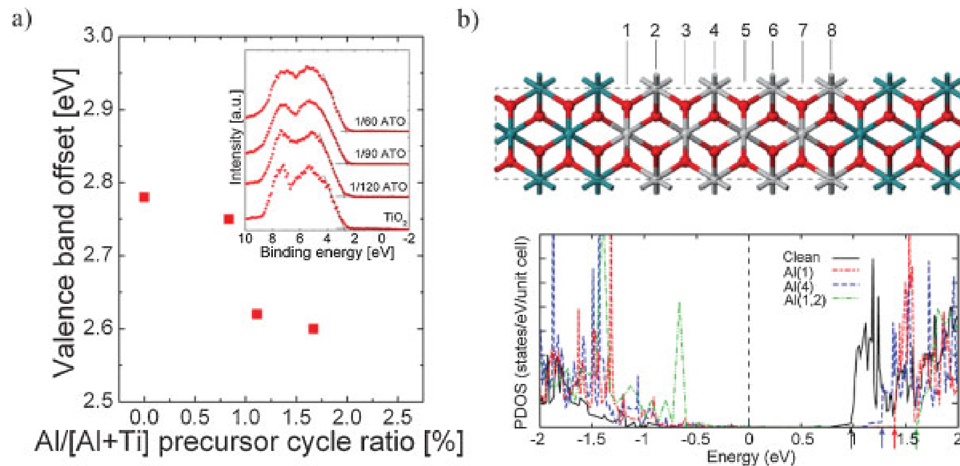

Figure 5. (a) The variation in the valence band offset as a function of the Al/[Al+Ti] precursor cycle ratio. Inset figure shows valence band spectra of TiO_2 and ATO films with various R_{pc} measured by XPS. (b) The side view of the unit cell of the model system for first-principles calculations. TiO_2 layer is sandwiched between metallic electrodes of RuO_2. Also shown in (b) is the partial density of states (PDOS) projected onto 5th layer of TiO_2 for various cases of Al doping. The number in parentheses indicates the layer where the Al atoms are doped. The Fermi level is set to zero in all cases (vertical dashed line).

1.54 eV, respectively (inset figure of Fig. 4d). Therefore, it can be understood that the large reduction in the leakage current density induced by the Al-doping is due to the increase in the Schottky barrier height by ~0.5 eV. The reason for the increase in Φ_b caused by the Al-doping was investigated by XPS and first principles calculations, as shown below.

The energy loss of the photoelectrons in the XPS spectra caused by the scattering with the valence electrons gives information about the valence band structure of the TiO_2 and ATO films. The energy cut-off level of the photoelectrons provides information on the Fermi levels (E_F). Therefore, the energy distance between E_F and the upper edge of the valence band (E_V) and, thus, the distance between E_F and the lower edge of the conduction band (E_C) can be obtained from the known band gap (E_g) once the XPS valence band spectra have been obtained. The inset figure of Figure 5a shows the XPS valence band spectra of the TiO_2 and ATO films with R_{pc} values of 1/∞, 1/120, 1/90, and 1/60. The corresponding E_F–E_V values are 2.78, 2.75, 2.62, and 2.60 eV, respectively, as shown in Figure 5a. Therefore, it can be understood that the Al- doping shifts the E_F toward E_V by ~0.2 eV. This is consistent with the original idea that the Al functions as an acceptor in TiO_2. The large E_F–E_V value (2.78 eV) of TiO_2 compared to the ideal value (1.55 eV) suggests that the TiO_2 film has an n-type nature. Therefore, the Al-doping may increase the conduction band offset, viz. Φ_b, of the Pt/TiO_2. The apparent inconsistency between the electrically extracted increase in Φ_b (~0.5 eV) and the value obtained by XPS (~0.2 eV) can be understood as follows. The E_F–E_V values obtained from the XPS spectra correspond to the free surfaces of the TiO_2 or ATO films which are influenced by the surface states, contaminants, etc. When Pt comes into contact with the dielectric films, various quantum-mechanical and electrochemical interactions occur and, thus, the interface states are influenced. Therefore, Φ_b could be different from E_F–E_V obtained by XPS. However, the relatively larger Φ_b of Pt/ATO compared to that of Pt/TiO_2 would be expected to be maintained.

The microscopic origin of the increase in Φ_b was investigated by first-principles calculations based on the density functional methods.[27,28] In Figure 5b, the model system consisting of a series of TiO_2 and RuO_2 layers is shown. For the convenience of modeling, RuO_2 instead of a Pt electrode was investigated in this calculation. However, the generality of the results described below reflects the fact that the explanation based on the same mechanism will be valid for both electrodes. The in-plane lattice parameters are set to those of crystalline TiO_2 in the rutile phase. One or two Ti atoms in certain layers are replaced with Al atoms and the atomic positions are relaxed until the Hellmann-Feynman forces are reduced to within 0.03 eV $Å^{-1}$. The total energy with respect to the position of the doping site is calculated and it is found that Al doping is more stable at the interface by 0.15 or 0.25 eV. This is explained by the image-charge interaction with the metal electrodes induced by charged defects. The substantial binding energy at the interface indicates that Al atoms may segregate around the interface region with a density much higher than the average doping concentration. This is in good agreement with the experimental observations shown in Figure 2a. In Figure 5b, the partial densities of states (PDOS) projected onto the middle TiO_2 layer are plotted. As a reference, the PDOS for the clean interface is also displayed. It is found that the conduction band offset substantially changes on Al doping. When one Al atom is replaced [Al(1) and Al(4) in Fig. 5b], which corresponds to a doping concentration of 12.5%, the offset increases from 1 eV to 1.25 or 1.4 eV depending on the doping position. If two Al atoms are doped at the first and fourth interfacial layers [Al(1,2) in Fig. 5b; doping concentration of 25%], the offset further increases to 1.65 eV. The change in the Schottky barrier of 0.65 eV is in a close agreement with the experimental value of 0.5 eV at the optimal

 © 2008 WILEY-VCH Verlag GmbH & Co. KGaA,Weinheim

leakage behaviors, indicating that the interfacial region would be heavily doped with Al dopants. The origin of the variations in Φ_b can be understood based on the charge transfer between the dielectrics and metal electrodes. Due to their nominal valence state of +3, the Al atoms in TiO_2 act as acceptors, as discussed above. When in contact with metal electrodes with a work function smaller than that for TiO_2 (7.1 eV, equal to the sum of the energy gap and affinity), the electron flows from the metals to the acceptor levels at the interface region. The direction of the induced dipole moment is such that the Fermi level of the electrodes effectively shifts down toward the valence edge of TiO_2, which is consistent with the ab initio results. In passing, it has to be said that the energy gap of TiO_2 is underestimated within our density functional method and therefore the relative shift is more reliable than the absolute values of Φ_b. In addition, the shift in band offsets by Al dopants originated from the band bending induced by charged dopants and therefore should be insensitive to the choice of exchange-correlation functionals. On the other hand, the energy gap of Al_2O_3 (8.8 eV) is much higher than that of TiO_2, and therefore the possibility of increase in the E_g of TiO_2 by Al-doping has to be addressed because it can also increase Φ_b. From the previous report[29] and the authors' own ab initio calculations, it is expected that the E_g increases by $\leq$0.1 eV when the Al-doping concentration is 10–20%. Although 0.1 eV is not insignificant in reducing the leakage current, this value is still much smaller than the experimentally observed increase in the Φ_b ($\sim$0.5 eV). Therefore, it is concluded that the significant decrease in the leakage current was induced by the Fermi level shift, rather than by the increase of the energy gap.

The work described herein concerns the development of capacitor dielectrics of DRAMs with sub-40 nm design rules. The incorporation of Al ions into the TiO_2 films made it possible to achieve a dielectric film with a minimum t_{ox} of 0.48 nm, while still guaranteeing a low enough leakage current. This value is the lowest among the reported t_{ox} values ever since the mass-production of compatible simple binary oxides began. The conformity of the ATO films on 3D structured capacitors was also confirmed (see Supporting Information).

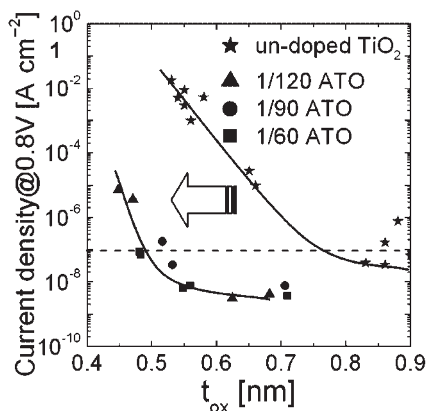

Figure 6. Overall summary of the leakage current density at the applied voltage of 0.8 V versus t_{ox} for the TiO_2 and Al-doped TiO_2 thin films.

Since the 3D conformal ALD processes of Al_2O_3 and TiO_2 have been well developed and all of the consumables involved are quite inexpensive, the fabrication process of ATO films at a mass-production compatible level may not add any significant burden to the present DRAM capacitor fabrication process. The required process temperature is also low enough to ensure the structural and electrical stability of the bottom electrode and underlying semiconductor devices. Figure 6 shows the overall summary plot of the J (at 0.8 V) versus t_{ox} of the TiO_2 and Al-doped TiO_2 thin films. As discussed previously, the proper Al-doping reduced the J level by $\sim 10^5$ times at a t_{ox} of approximately $\sim$0.5 nm. As a final comment, the exact doping concentration of Al in the range shown in this report does not significantly matter. Figure 6 reveals that the data points obtained from the films with the different Al-doping concentrations (R_{pc}) aligned on a single line, implying that the lower doping concentrations also result in the improvement in the leakage performance. This is another key merit of this process, when considering the inherent process variation in mass-production.

In conclusion, Al-doped TiO_2 thin films to be used in future DRAM capacitors with excellent leakage properties as well as high dielectric constants are fabricated. The microscopic mechanism to lower the leakage current was adjusting the Fermi level to the mid-gap position. Increase of the energy gap by the Al-doping was expected to be less than 0.1 eV, therefore its influence on the leakage current might be negligible. Although this work was motivated by the application of the material to DRAM, the results are also applicable to other applications, such as thin films type multi-layer ceramic capacitor (MLCC) or thin film capacitor in system-on-plastic (or printed circuit board).

Experimental

TiO_2 and ATO films were deposited using a traveling-wave type ALD reactor on sputtered Ru(30 nm)/Ta_2O_5(8 nm)/SiO_2/(100 nm)/Si substrates at a wafer temperature of 250 °C. $Ti(OC_3H_7)_4$ and $Al(CH_3)_3$ were used as the Ti and Al precursors, respectively, and O_3 with a concentration of 390 gm^{-3} was used as the oxidant. In order to incorporate Al ions into the films, an Al-O layer was inserted discretely into the film by substituting one Ti-O cycle with an Al-O cycle. The concentration of Al in the films was controlled by varying the Al and Ti precursor cycle ratio (R_{pc}, [number of Al-O cycle]/[number of Al-O cycle + number of Ti-O cycles]). The ATO film thickness was controlled by adjusting the number of super-cycles. A super-cycle was composed of n cycles of TiO_2 and one cycle of Al_2O_3. The cycle of Al_2O_3 was inserted two-thirds of the way through a super-cycle. R_{pc} was varied in order to change the Al concentration in the films. The film thickness was measured by ellipsometry, X-ray reflectivity, and cross-section HRTEM. XPS was used to investigate the chemical binding states and valence band spectra of the films. The film compositions of the films and carbon concentration in the film were investigated by inductively coupled plasma spectroscopy and Auger electron spectroscopy depth profiling. For the electrical measurement, MIM capacitors were fabricated using sputtered Pt through a shadow mask as the top electrode. The fabricated MIM capacitors were annealed at 400 °C under an N_2 (95%)/O_2 (5%) atmosphere. The C–V and J–V characteristics were measured using a Hewlett-Packard 4194

© 2008 WILEY-VCH Verlag GmbH & Co. KGaA,Weinheim

impedance analyzer at 10 kHz and a Hewlett-Packard 4140 picoammeter/voltage source.

Received: May 5, 2007
Revised: December 5, 2007
Published online: March 20, 2008

[1] A. I. Kingon, J.-P. Maria, S. K. Steriffer, *Nature* **2000**, *406*, 1032.
[2] H. Schroeder, A. Kingon, in *Nanoelectronics and Information Technology*, (Ed: R. Waser), WILEY-VCH, Weinheim, Germany **2003**, Chap. IV.
[3] J. F. Scott, C. A. Auraujo, B. M. Melnick, L. D. McMillan, R. Zuleeg, *J. Appl. Phys.* **1991**, *70*, 382.
[4] P. Balk, *Adv. Mater.* **1995**, *7*, 703.
[5] Y. Aoki, T. Ueda, H. Shirai, T. Sakoh, T. Kitamura, S. Arai, M. Sakao, K. Inoue, M. Takeuchi, H. Sugimura, M. Hamada, T. Wake, I. Naritake, T. Lizuka, T. Yamamoto, K. Ando, K. Noda, *IEDM Tech. Dig.* **2002**, *831.*
[6] S.-J. Won, Y.-K. Jeong, D.-J. Kwon, M.-H. Park, H.-K. Kang, K.-P. Suh, H.-K. Kim, J.-H. Ka, K.-Y. Yun, D.-H. Lee, D.-Y. Kim, Y.-M. Yoo, C.-S. Lee, *Symp. on VLSI. Tech. Dig.* **2003**, *23.*
[7] K. R. Yoon, K. V. Im, J. H. Yeo, E. A. Chung, Y. S. Kim, C. Y. Yoo, S. T. Kim, U. I. Chung, J. T. Moon, *SSDM Ext. Abst.* **2002**, *188.*
[8] K. Kim, *Microelectron. Reliab.* **2000**, *40*, 191.
[9] S. Ezhilvalavan, T.-Y. Tseng, *J. Appl. Phys.* **1998**, *83*, 4797.
[10] Semiconductor Industry Association, *The international technology roadmap for semiconductors (ITRS) 2005 edition and 2006 update* http://www.itrs.net/
[11] J. Nakahira, M. Kiyotoshi, S. Yamazaki, M. Nakabayashi, S. Niwa, K. Tsunoda, J. Lin, A. Shimada, M. Izuha, T. Aoyama, H. Tomita, K. Eguchi, K. Hieda, *Symp. on VLSI. Tech. Dig.* **2000**, *104.*
[12] C. S. Kang, C. S. Hwang, H.-J. Cho, B. T. Lee, S. O. Park, J. W. Kim, H. Horii, S.-I. Lee, Y. B. Koh, M.-Y. Lee, *Jpn. J. Appl. Phys. Part 1* **1996**, *35*, 4890.
[13] C. S. Hwang, *Mat. Sci. Eng. B* **1998**, *56*, 178.
[14] C. S. Hwang, S. O. Park, C. S. Kang, H. J. Cho, H. K. Kang, S. I. Lee, M. Y. Lee, *Appl. Phys. Lett.* **1995**, *67*, 2819.
[15] S. K. Kim, W.-D. Kim, K.-M. Kim, C. S. Hwang, J. Jeong, *Appl. Phys. Lett.* **2004**, *85*, 4112.
[16] M. Osada, Y. Ebina, H. Funakubo, S. Yokoyama, T. Kiguchi, K. Takada, T. Sasaki, *Adv. Mater.* **2006**, *18*, 1023.
[17] S. K. Kim, G. W. Hwang, W.-D. Kim, C. S. Hwang, *Electrochem. Solid-State Lett.* **2006**, *9*, F5.
[18] S. K. Kim, K.-M. Kim, O. S. Kwon, S. W. Lee, C. B. Jeon, W. Y. Park, C. S. Hwang, J. Jeong, *Electrochem. Solid-State Lett.* **2005**, *8*, F59.
[19] S. K. Kim, S. Y. Lee, S. W. Lee, G. W. Hwang, C. S. Hwang, J. W. Lee, J. Jeong, *J. Electrochem. Soc.* **2007**, *154*, D95.
[20] J. Robertson, *J. Vac. Sci. Technol. B* **2000**, *18*, 1785.
[21] A. Von Richthofen, R. Cremer, R. Domnick, D. Neuschütz, *Thin Solid Films* **1998**, *315*, 66.
[22] Y. B. Zheng, S. J. Wang, A. C. H. Huan, C. Y. Tan, L. Yan, C. K. Ong, *Appl. Phys. Lett.* **2005**, *86*, 112910.
[23] M. Stengel, N. A. Spaldin, *Nature* **2006**, *443*, 679.
[24] K. Natori, D. Otani, N. Sano, *Appl. Phys. Lett.* **1998**, *73*, 632.
[25] C. T. Black, J. J. Welser, *IEEE Trans. Electron Devices* **1999**, *46*, 776.
[26] C. S. Hwang, *J. Appl. Phys.* **2002**, *92*, 432.
[27] a) G. Kresse, J. Hafner, *Phys. Rev. B* **1993**, *47*, 558. b) G. Kresse, J. Hafner, *Phys. Rev. B* **1994**, *49*, 14251.
[28] D. M. Ceperley, B. J. Alder, *Phys. Rev. Lett.* **1980**, *45*, 566.
[29] M. M. Islam, T. Bredow, A. Gerson, *Phys. Rev. B* **2007**, *76*, 045217.

© 2008 WILEY-VCH Verlag GmbH & Co. KGaA,Weinheim